

Unveiling a Novel, Cation-Rich Compound in a High-Pressure Pb–Te Binary System

Hulei Yu,^{†,‡} Xiaohuan Lin,[§] Kuo Li,^{*,§} and Yue Chen^{*,†,‡}

HPSTAR
749-2019

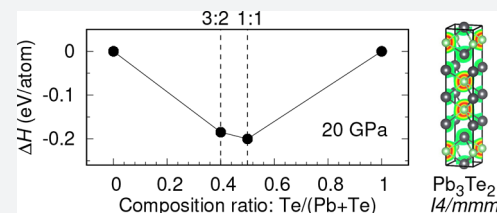
[†]Department of Mechanical Engineering, The University of Hong Kong, Pokfulam Road, Hong Kong SAR, China

[‡]HKU Zhejiang Institute of Research and Innovation, 1623 Dayuan Road, Lin An 311305, China

[§]Center for High Pressure Science and Technology Advanced Research, 10 Dongbeiwang West Road, Haidian, Beijing, China

Supporting Information

ABSTRACT: Because of the common oxidation states of group IV elements (+2 or +4) and group VI elements (−2), 1:1 and 1:2 are two typical stoichiometries found in the IV–VI compounds. Particularly, in the Pb–Te binary system, the 1:1 stoichiometric PbTe is believed to be the only stable compound. Herein, using evolutionary algorithms, density functional theory, a laser-heated diamond anvil cell, and synchrotron X-ray diffraction experiments, we discovered a novel Pb–Te compound with an unexpected stoichiometry of 3:2 above 20 GPa. This tetragonal Pb₃Te₂ is the one of the very few cation-rich compounds that has ever been discovered in the entire IV–VI binary system. Further analyses based on electron density distribution, electron localization function, and Bader charge have shown that this newly discovered compound has a mixed character of chemical bonding with a decreased ionicity. By further calculating the electron–phonon interaction, Pb₃Te₂ is predicted to exhibit a superconducting transition at low temperatures. The discovery of Pb₃Te₂ paves the way for further explorations of other novel cation-rich IV–VI group compounds.



INTRODUCTION

Lead telluride (PbTe) is one of the most representative semiconductors in the IV–VI group compounds, and it attracts much research interest due to its outstanding thermoelectric and photovoltaic properties.^{1–3} As Pb has an oxidation state of +2 or +4 and tellurium has a −2 oxidation state, compounds with 1:1 and 1:2 stoichiometries are expected to exist in the Pb–Te binary system. At ambient conditions, only the 1:1 stoichiometric PbTe compound has been observed.⁴ The PbTe compound has a rocksalt B1 crystal structure with a narrow band gap and does not show any temperature-induced phase transition below the melting point.^{5,6} By exerting a hydrostatic pressure of approximately 6 GPa, PbTe undergoes a structural phase transition into an orthorhombic structure with a space group of *Pnma* (β -FeB prototype).^{7,8} At a higher pressure above 13 GPa, PbTe transforms into the body-centered cubic B2 phase (*Pm* $\bar{3}$ *m* space group),⁹ which was reported to have a superconducting transition temperature of \sim 8 K at 17.5 GPa.¹⁰

The properties of materials may be significantly altered under high pressures,^{11,12} in which new compounds that do not exist at ambient conditions may be synthesized.^{12–14} The first-principles evolutionary algorithm is a recently developed method for exploring ground-state crystal structures, and it has been shown to be extremely successful in the studies of high-pressure phase transitions.¹⁵ Using this approach, Zhang et al. predicted the existence of various sodium chloride compounds with counterintuitive stoichiometries under high pressures, and the predictions were further confirmed in experiments.¹⁶ Dong et al. recently reported a novel Na₂He compound with a fluorite-type crystal structure above 113 GPa¹⁷ based on

evolutionary structural searches. Our previous work also unveiled a new superconducting Sn₃Se₄ compound under high pressures.¹⁸

In this work, we systematically investigate the Pb–Te system under hydrostatic pressures up to 40 GPa by combining density functional theory (DFT) and evolutionary algorithms. In addition to the well-known PbTe compound, a novel, cation-rich compound, Pb₃Te₂, is predicted to be both energetically preferable and dynamically stable at high pressures. Subsequent synthesis of Pb₃Te₂ was conducted in a laser-heated diamond anvil cell (DAC). Bader charge and electron localization function were also calculated to study its diverse atomic bonding. Furthermore, the electronic band structures and electron–phonon interaction were also calculated, and it was found that Pb₃Te₂ exhibits a lower superconducting transition temperature comparing to PbTe.

RESULTS AND DISCUSSION

The results of our structural search for stable Pb–Te compounds are shown in Figure 1a. At pressures below 10 GPa, there is only one compound (PbTe) that appears on the convex hulls and is energetically preferable. As expected, PbTe undergoes a structural phase transition from the rocksalt *Fm* $\bar{3}$ *m* (B1) structure through the β -FeB type *Pnma* structure to a higher symmetry *Pm* $\bar{3}$ *m* (B2) structure with increasing pressure. The computed phase transition pressures from *Fm* $\bar{3}$ *m* to *Pnma* and from *Pnma* to *Pm* $\bar{3}$ *m* are 9 and 13 GPa,

Received: January 25, 2019

Published: April 9, 2019

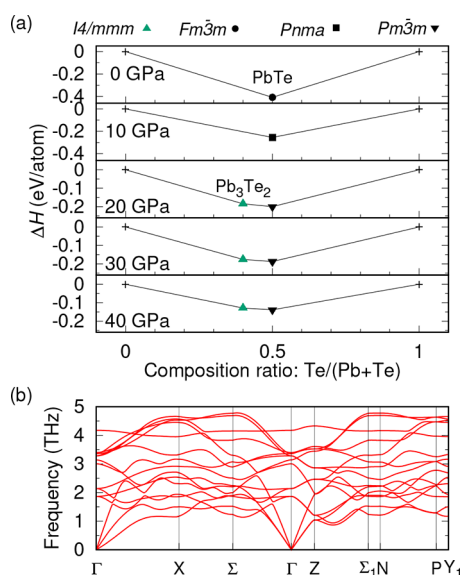


Figure 1. (a) Enthalpies of formation of the predicted stable compounds in the Pb–Te binary system. Solid lines represent the convex hulls at different hydrostatic pressures. (b) Phonon dispersions of the predicted Pb_3Te_2 compound calculated at a hydrostatic pressure of 20 GPa using the small displacement method.

respectively; the experimental phase transition pressures are 6 and 13 GPa, respectively.^{7,9} Therefore, the predicted pressure-induced phase transition path and the corresponding phase transition pressures are in good agreement with experimental results, indicating the reliability of our calculations. More importantly, a novel compound with a counterintuitive stoichiometry of 3:2 is found to become energetically stable at 20 GPa. This unexpected Pb_3Te_2 is predicted to have a space group of $I4/mmm$ and to remain energetically preferable up to the highest pressure 40 GPa studied in this work.

In addition to the energetics, phonon calculations have also been performed to investigate the dynamical stability of Pb_3Te_2 . It is seen from the phonon dispersions shown in Figure 1b that no imaginary phonon frequencies are observed in Pb_3Te_2 at 20 GPa, suggesting that the lattice is dynamically stable. On the basis of the enthalpy and phonon calculations, Pb_3Te_2 is predicted to be both energetically and dynamically stable at pressures above 20 GPa. The tetragonal crystal structure of Pb_3Te_2 belongs to the Os_2Al_3 prototype, which is most commonly observed in compounds formed between metallic elements and in high-pressure oxides.¹⁹ All Te atoms in Pb_3Te_2 are in equivalent lattice sites, and each Te atom has eight nearest neighbor Pb atoms, which is similar to that in the B2 phase of PbTe. On the other hand, there are two nonequivalent Pb lattice sites (denoted as Pb1 and Pb2) in Pb_3Te_2 with either four or eight nearest neighbor Te atoms. The predicted Wyckoff positions of Pb1, Pb2 and Te are $4e$ (0, 0, 0.8), $2a$ (0,0,0), and $4e$ (0, 0, 0.4), respectively.

The relatively large pressure range where Pb_3Te_2 is predicted to be stable suggests it is possible to further synthesize the compound. To verify our prediction, corresponding high-pressure experiments were performed. Figure 2 shows the Rietveld refinement result of the Pb–Te system at about 20 GPa and 1315 K. The characteristic peaks of the predicted Pb_3Te_2 compound can be clearly identified on the synchrotron X-ray diffraction (XRD) patterns. The nonfitted peaks may be attributed to the formation of unidentified

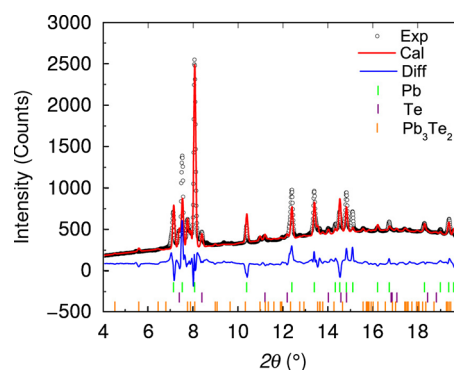


Figure 2. Rietveld refinement of Pb–Te binary system under 20 GPa and 1315 K. The experimental and calculated data are shown in black circles and red solid curve, respectively; their difference is shown in blue curve. The Bragg positions of Pb, Te, and Pb_3Te_2 are indicated by green, purple, and orange vertical bars, respectively.

metastable phases during laser heating. The refined lattice parameters from the XRD data are $a = 3.60$ Å and $c = 17.68$ Å, and the space group is $I4/mmm$. The experimental results are in good agreement with our predictions; the theoretical lattice parameters at 20 GPa and 0 K are $a = 3.69$ Å and $c = 17.80$ Å. Because of the typical oxidation states of group IV and VI elements, the binary compounds usually have 1:1 or 1:2 stoichiometries. Therefore, the successful synthesis of the counterintuitive Pb_3Te_2 compound indicates the discovery of another rare cation-rich compound in the important IV–VI binary system.

To better understand the formation of Pb_3Te_2 , we further analyzed its atomic bonding. From the calculations of Bader charge²⁰ (see Table 1), it is seen that in rocksalt $Fm\bar{3}m$ PbTe,

Table 1. Bader Charge Analysis on Different Pb–Te Compounds

	P (GPa)	Pb (e)	Te (e)
Pb_3Te_2	20	0.28 (Pb1)	−0.52
		0.48 (Pb2)	
$Pm\bar{3}m$ PbTe	20	0.51	−0.51
$Fm\bar{3}m$ PbTe	0	0.67	−0.67

each Pb atom donates 0.67 electron to Te at 0 GPa. As the pressure increases to 20 GPa, fewer electrons are transferred between Pb and Te atoms in the stable $Pm\bar{3}m$ PbTe phase and the Pb_3Te_2 compound. Additionally, it is also noticed that the numbers of electrons donated by the nonequivalent Pb atoms in Pb_3Te_2 are different, which may be related to the different nearest neighbor atomic environments. The decrease of electron transfer between Pb and Te atoms under pressures suggests a weakening ionic character of $Pm\bar{3}m$ PbTe and Pb_3Te_2 .

It is seen from Figure 3a that the crystal structure of Pb_3Te_2 contains building blocks similar to those of the $Pm\bar{3}m$ PbTe but has a different stacking order. By calculating the electron localization function (ELF), we observe localized electrons around both Pb and Te atoms in the semiconducting $Fm\bar{3}m$ PbTe at 0 GPa, whereas the electrons around Te atoms become more delocalized in Pb_3Te_2 and $Pm\bar{3}m$ PbTe at 20 GPa. The sphere-like ELF isosurfaces around Pb2 atoms, which locate between two Te atomic layers, are similar to those of $Pm\bar{3}m$ PbTe, while the isosurfaces around Pb1 atoms

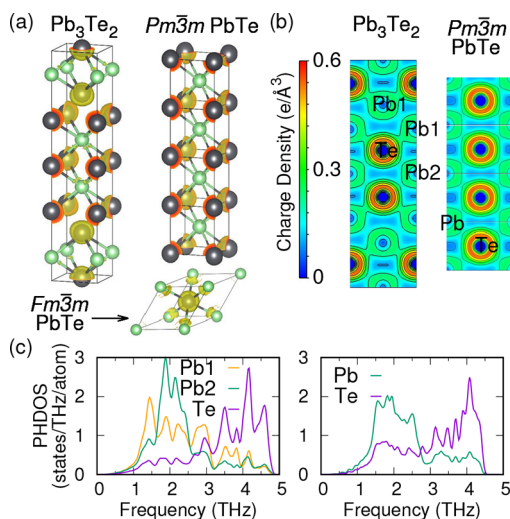


Figure 3. (a) Electron localization function of Pb_3Te_2 at 20 GPa, $Pm\bar{3}m$ PbTe at 20 GPa, and $Fm\bar{3}m$ PbTe at 0 GPa. Pb and Te atoms are shown in black and green spheres, respectively. The ELF isosurface value is equal to 0.85. (b) Charge density distributions on the (110) planes of Pb_3Te_2 and $Pm\bar{3}m$ PbTe at 20 GPa. (c) Projected phonon DOS of Pb_3Te_2 (left) and $Pm\bar{3}m$ PbTe (right) at 20 GPa.

located between one Pb atomic layer and one Te atomic layer are more anisotropic. We attribute the delocalization of electrons around Te in Pb_3Te_2 to the reduced lattice parameters as it is seen from Figure S2 (Supporting Information) that these electrons are more localized at 0 GPa. It is also notable that the charge density distribution is directional in Pb_3Te_2 (see Figure 3b). The charge density distribution and the bond length between Pb2 and Te ($L_{\text{Pb2-Te}} = 3.19 \text{ \AA}$) in Pb_3Te_2 are similar to those between Pb and Te in $Pm\bar{3}m$ PbTe ($L_{\text{Pb-Te}} = 3.16 \text{ \AA}$). The slightly shorter bond length between Pb1 and Te ($L_{\text{Pb1-Te}} = 3.10 \text{ \AA}$) in Pb_3Te_2 leads to a larger charge density. On the other hand, the more diverse bonding environment around the Pb1 atom leads to a wider and more evenly distributed projected phonon density of states (PHDOS), as shown in Figure 3c. The projected PHDOS onto the Pb2 atoms mostly locate between 1.5 and 2.5 THz, which is more similar to that of the Pb atoms in $Pm\bar{3}m$ PbTe . Therefore, the projected PHDOS is consistent with the analysis of the atomic bonding environment.

The electronic band structures and density of states (DOS) of the different Pb–Te compounds have also been computed under high pressures. As shown in Figure 4a, Pb_3Te_2 does not have a band gap at 20 GPa, suggesting a metallic state. The Fermi level is located near a pseudogap, which may imply a higher stability^{21,22} and a character of covalent bonding.²³ From the projected DOS, it is found that the DOS at the Fermi level is mainly contributed by the Pb1 and Pb2 4p states. The majority of the electronic states below Fermi level are the Te 5p states. On the other hand, $Pm\bar{3}m$ PbTe is also metallic with a gapless band structure at 20 GPa, as shown in Figure 4b. Different from Pb_3Te_2 , the largest contribution to DOS at the Fermi level comes from the Te 5p states. The projected DOS of Pb_3Te_2 and $Pm\bar{3}m$ PbTe near the Fermi level are rather similar, whereas there is an upward shift of Fermi energy in Pb_3Te_2 due to the higher concentration of Pb that donates electrons.

It was reported that PbTe goes through a superconducting transition at high pressures;¹⁰ therefore, we have further

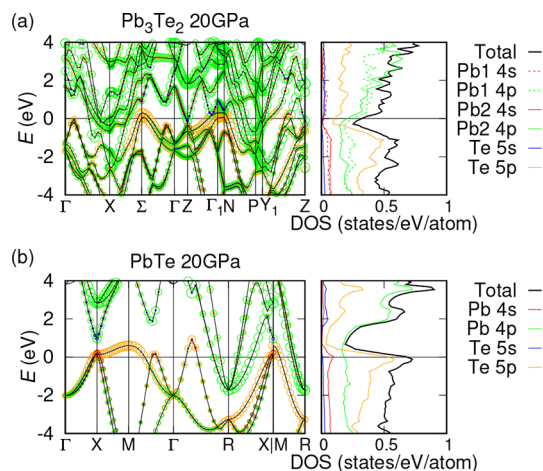


Figure 4. Projected electronic band structures along high symmetry paths (left) and projected DOS (right) of Pb_3Te_2 (a) and $Pm\bar{3}m$ PbTe (b) at 20 GPa. Fermi level is located at 0 eV. Different circle sizes correspond to the projected weights of different orbitals.

studied the electron–phonon coupling in the newly synthesized Pb_3Te_2 compound. It is seen from Figure 5 that the

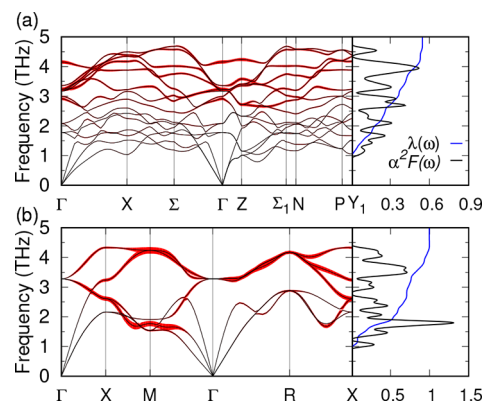


Figure 5. Phonon dispersions, phonon linewidths due to electron–phonon interaction, Eliashberg spectral functions $\alpha^2F(\omega)$, and the integrated electron–phonon coupling parameters $\lambda(\omega)$ of Pb_3Te_2 (a) and $Pm\bar{3}m$ PbTe (b), as calculated from DFPT at 20 GPa.

optical phonon modes of Pb_3Te_2 in the range of 2.5–5 THz have larger linewidths (i.e., shorter lifetimes) compared to the lower-frequency modes, suggesting the higher-frequency modes have stronger coupling to the electrons. On the other hand, the optical and acoustic phonons above 1 THz in the high-pressure $Pm\bar{3}m$ phase of PbTe have larger linewidths than the lower-frequency acoustic phonons near the Brillouin zone center. The phonon linewidths of Pb_3Te_2 are generally smaller than those of $Pm\bar{3}m$ PbTe ; therefore, the total EPC parameter of Pb_3Te_2 at 20 GPa ($\lambda = 0.55$) is also smaller than that of $Pm\bar{3}m$ PbTe ($\lambda = 1.00$). As a result, the smaller λ leads to a lower superconducting transition temperature of Pb_3Te_2 ($T_c = 1.1\text{--}2.0 \text{ K}$) than that of $Pm\bar{3}m$ PbTe ($T_c = 5.76\text{--}7.10 \text{ K}$). This lower T_c value may also be correlated to the lower DOS at the Fermi level of Pb_3Te_2 at 20 GPa (see Figure 4).

CONCLUSIONS

In summary, we have performed first-principles evolutionary structural searches for new Pb–Te compounds under hydrostatic pressures up to 40 GPa. A novel, cation-rich compound

with an unconventional stoichiometry of 3:2 is predicted to be stable above 20 GPa from enthalpy and phonon calculations. The prediction is further verified through laser-heated DAC experiments with synchrotron X-ray diffraction. The novel Pb_3Te_2 compound has a tetragonal crystal structure with a space group of $I4/mmm$. Atomic bonding analysis unveils a decreased ionicity and a more delocalized electron distribution in Pb_3Te_2 . The electronic band structure and electron–phonon coupling calculations show that Pb_3Te_2 is metallic and has a low superconducting transition temperature under pressures. Our discovery paves the way for further explorations of other potentially hidden, cation-rich IV–VI group compounds with counterintuitive stoichiometries.

■ COMPUTATIONAL SECTION

Variable-composition structural searches under hydrostatic pressures based on first-principles evolutionary algorithm were performed by using USPEX and VASP.^{24,25} A maximum number of 16 atoms was allowed in a unit cell during the structural searches. New generations of crystal structures were created through heredity (40%), random (20%), lattice mutation (20%), and transmutation (20%) based on the best 60% crystal structures in the previous generations. Structural relaxations and electronic property calculations were performed in the framework of the projector-augmented wave (PAW) method²⁶ using the generalized gradient approximation (GGA) and the Perdew–Burke and Ernzerhof (PBE) functional²⁷ with $6s^26p^2$ and $5s^25p^4$ as the valence electrons of Pb and Te, respectively. A plane-wave energy cutoff of 350 eV, a Γ -centered k -point grid of $0.03 \times 2\pi \text{ \AA}^{-1}$, and a convergence criterion of 10^{-6} eV were applied in the electronic self-consistent calculations. Phonon dispersions were computed using the small displacement method²⁸ with a $3 \times 3 \times 3$ supercell of Pb_3Te_2 ; for more accurate atomic forces, the total energy convergence criterion was increased to 10^{-8} eV, and a higher cutoff energy of 450 eV was used. Density functional perturbation theory (DFPT) as implemented in Quantum-Espresso²⁹ has been used to calculate the electron–phonon coupling (EPC) with norm-conserving pseudopotentials.³⁰ An 80 Ry cutoff energy was utilized in EPC calculations with a $4 \times 4 \times 4q$ -point mesh and a $16 \times 16 \times 16k$ -sampling. The Gaussian broadening was set to 0.03 Ry. Interpolation over the Brillouin zone was adopted to obtain the electron–phonon coefficient λ .³¹ Superconducting transition temperature (T_c) was computed using the Allen–Dynes modified McMillan equation³² with typical values of the Coulomb pseudopotential μ^* (0.1–0.14).

■ EXPERIMENTAL SECTION

We loaded the reactant (Pb and Te powder mixed with a molar ratio of 3:2) into a symmetric DAC equipped with Boehler-type diamonds and stainless steel gaskets. The diameter of the diamond culets is approximately 300 μm , and the cell opening angle is about 42° (4θ). Ne was loaded as the pressure medium and thermal insulator. In situ laser heating and XRD experiment were carried out at HPCAT 16-ID-B, Advanced Photon Source, Argonne National Lab. The sample was compressed to 20.0 GPa as calibrated by Ruby and then heated by two identical IPG YLR-100-1064-WC fiber lasers on both sides. The diameter of the laser spot is 40–50 μm . In situ XRD data were collected 5–10 s after the laser power was increased. The incident X-ray was monochromated

to a wavelength of 0.3445 Å , and the beam size was $\sim 10 \mu\text{m}$. Mar165CCD was used as the detector. Each data collection lasted for 3 s, and laser power was increased when the repeated data looked the same as the previous one. Rietveld refinement was conducted by JANA2006.^{33,34}

Safety Statement. No unexpected or unusually high safety hazards were encountered.

■ ASSOCIATED CONTENT

📄 Supporting Information

The Supporting Information is available free of charge on the ACS Publications website at DOI: 10.1021/acscentsci.9b00083.

Convex hull of Pb–Te binary system calculated from DFT at 20 GPa (Figure S1); predicted lattice parameters of potential metastable phases in the Pb–Te binary system at 20 GPa (Table S1); predicted lattice parameters of different phases at selected pressures (Table S2); electron localization function of Pb_3Te_2 at 0 GPa (Figure S2) (PDF)

■ AUTHOR INFORMATION

Corresponding Authors

*(K.L.) E-mail: likuo@hpstar.ac.cn.

*(Y.C.) E-mail: yuechen@hku.hk.

ORCID

Hulei Yu: 0000-0002-8689-6586

Kuo Li: 0000-0002-4859-6099

Yue Chen: 0000-0001-5811-6936

Notes

The authors declare no competing financial interest.

■ ACKNOWLEDGMENTS

This work is supported by the Research Grants Council of Hong Kong under Project Numbers 27202516, 17200017, and 17300018, and the National Natural Science Foundation of China under Project Numbers 51706192, 11874313, and 21771011. The authors are grateful for the research computing facilities offered by ITS, HKU, and the synchrotron radiation facilities at beamline 16-ID-B, Advanced Photon Source (APS), and SPring-8 (2017B1053).

■ REFERENCES

- (1) Tan, G.; Shi, F.; Hao, S.; Zhao, L.-D.; Chi, H.; Zhang, X.; Uher, C.; Wolverton, C.; Dravid, V. P.; Kanatzidis, M. G. Non-equilibrium processing leads to record high thermoelectric figure of merit in PbTe-SrTe . *Nat. Commun.* **2016**, *7*, 12167.
- (2) Böhm, M. L.; Jellicoe, T. C.; Tabachnyk, M.; Davis, N. J.; Wisnivesky-Rocca-Rivarola, F.; Ducati, C.; Ehrler, B.; Bakulin, A. A.; Greenham, N. C. Lead telluride quantum dot solar cells displaying external quantum efficiencies exceeding 120%. *Nano Lett.* **2015**, *15*, 7987–7993.
- (3) Heremans, J. P.; Jovovic, V.; Toberer, E. S.; Saramat, A.; Kurosaki, K.; Charoenphakdee, A.; Yamanaka, S.; Snyder, G. J. Enhancement of thermoelectric efficiency in PbTe by distortion of the electronic density of states. *Science* **2008**, *321*, 554–557.
- (4) Berchenko, N.; Fadeev, S.; Savchyn, V.; Kurbanov, K.; Trzyna, M.; Cebulski, J. Pb-Te-O phase equilibrium diagram and the lead telluride thermal oxidation. *Thermochim. Acta* **2014**, *579*, 64–69.
- (5) Bajaj, S.; Pomrehn, G. S.; Doak, J. W.; Gierlotka, W.; Wu, H.-j.; Chen, S.-W.; Wolverton, C.; Goddard, W. A.; Snyder, G. J. Ab initio study of intrinsic point defects in PbTe : an insight into phase stability. *Acta Mater.* **2015**, *92*, 72–80.

- (6) Dariel, M.; Dashevsky, Z.; Jarashnely, A.; Shusterman, S.; Horowitz, A. Carrier concentration gradient generated in p-type PbTe crystals by unidirectional solidification. *J. Cryst. Growth* **2002**, *234*, 164–170.
- (7) Rouse, G.; Klotz, S.; Saitta, A.; Rodriguez-Carvajal, J.; McMahon, M.; Couzinet, B.; Mezouar, M. Structure of the intermediate phase of PbTe at high pressure. *Phys. Rev. B: Condens. Matter Mater. Phys.* **2005**, *71*, 224116.
- (8) Demiray, F.; Berber, S. Ab initio investigation of B16 (GeS), B27 (FeB) and B33 (CrB/TlI) phases of lead chalcogenides. *Phys. Scr.* **2013**, *88*, 015603.
- (9) Chattopadhyay, T.; Werner, A.; Von Schnering, H.; Pannetier, J. Temperature and pressure induced phase transition in IV-VI compounds. *Rev. Phys. Appl.* **1984**, *19*, 807–813.
- (10) Brandt, N.; Gitsu, D.; Popovich, N.; Sidorov, V.; Chudinov, S. Superconductivity of the compounds PbTe and PbSe under high pressure. *Jetp Lett.* **1975**, *22*, 104–106.
- (11) Chi, Z.; Chen, X.; Yen, F.; Peng, F.; Zhou, Y.; Zhu, J.; Zhang, Y.; Liu, X.; Lin, C.; Chu, S.; Li, Y.; Zhao, J.; Kagayama, T.; Ma, Y.; Yang, Z. Superconductivity in pristine 2H_a-MoS₂ at ultrahigh pressure. *Phys. Rev. Lett.* **2018**, *120*, 037002.
- (12) Drozdov, A.; Erements, M.; Troyan, I.; Ksenofontov, V.; Shylin, S. Conventional superconductivity at 203 K at high pressures in the sulfur hydride system. *Nature* **2015**, *525*, 73.
- (13) Einaga, M.; Sakata, M.; Ishikawa, T.; Shimizu, K.; Erements, M. I.; Drozdov, A. P.; Troyan, I. A.; Hirao, N.; Ohishi, Y. Crystal structure of the superconducting phase of sulfur hydride. *Nat. Phys.* **2016**, *12*, 835.
- (14) Dalladay-Simpson, P.; Howie, R. T.; Gregoryanz, E. Evidence for a new phase of dense hydrogen above 325 gigapascals. *Nature* **2016**, *529*, 63.
- (15) Oganov, A. R.; Ma, Y.; Lyakhov, A. O.; Valle, M.; Gatti, C. Evolutionary crystal structure prediction as a method for the discovery of minerals and materials. *Rev. Mineral. Geochem.* **2010**, *71*, 271–298.
- (16) Zhang, W.; Oganov, A. R.; Goncharov, A. F.; Zhu, Q.; Bouffelfel, S. E.; Lyakhov, A. O.; Stavrou, E.; Somayazulu, M.; Prakapenka, V. B.; Konôpková, Z. Unexpected stable stoichiometries of sodium chlorides. *Science* **2013**, *342*, 1502–1505.
- (17) Dong, X.; et al. A stable compound of helium and sodium at high pressure. *Nat. Chem.* **2017**, *9*, 440.
- (18) Yu, H.; Lao, W.; Wang, L.; Li, K.; Chen, Y. Pressure-stabilized tin selenide phase with an unexpected stoichiometry and a predicted superconducting state at low temperatures. *Phys. Rev. Lett.* **2017**, *118*, 137002.
- (19) Zhang, Q.; Wu, X.; Qin, S. A nine-fold coordinated vanadium by oxygen in V₂O₃ from first-principles calculations. *Eur. Phys. J. B* **2012**, *85*, 267.
- (20) Tang, W.; Sanville, E.; Henkelman, G. A grid-based bader analysis algorithm without lattice bias. *J. Phys.: Condens. Matter* **2009**, *21*, 084204.
- (21) Ögüt, S.; Rabe, K. M. Band gap and stability in the ternary intermetallic compounds NiSnM (M= Ti, Zr, Hf): a first-principles study. *Phys. Rev. B: Condens. Matter Mater. Phys.* **1995**, *51*, 10443.
- (22) Feng, L.; Liu, E.; Zhang, W.; Wang, W.; Wu, G. First-principle investigation of electronic structure, magnetism and phase stability of Heusler-type Pt_{2-x}Mn_{1+x}Ga alloys. *J. Magn. Magn. Mater.* **2015**, *377*, 40–43.
- (23) Zhang, B.; Wu, L.; Li, Z. Predicted structural evolution and detailed insight into configuration correlation, mechanical properties of silicon-boron binary compounds. *RSC Adv.* **2017**, *7*, 16109–16118.
- (24) Lyakhov, A. O.; Oganov, A. R.; Valle, M. Crystal structure prediction using evolutionary approach. In *Modern Methods of Crystal Structure Prediction*; Wiley-Blackwell, 2010; Chapter 7, pp 147–180.
- (25) Kresse, G.; Furthmüller, J. Efficiency of ab-initio total energy calculations for metals and semiconductors using a plane-wave basis set. *Comput. Mater. Sci.* **1996**, *6*, 15–50.
- (26) Blöchl, P. E. Projector augmented-wave method. *Phys. Rev. B: Condens. Matter Mater. Phys.* **1994**, *50*, 17953–17979.
- (27) Perdew, J. P.; Burke, K.; Ernzerhof, M. Generalized gradient approximation made simple. *Phys. Rev. Lett.* **1996**, *77*, 3865–3868.
- (28) Togo, A.; Oba, F.; Tanaka, I. First-principles calculations of the ferroelastic transition between rutile-type and CaCl₂-type SiO₂ at high pressures. *Phys. Rev. B: Condens. Matter Mater. Phys.* **2008**, *78*, 134106.
- (29) Giannozzi, P.; et al. QUANTUM ESPRESSO: a modular and open-source software project for quantum simulations of materials. *J. Phys.: Condens. Matter* **2009**, *21*, 395502.
- (30) Semenov, D. V.; Kvashnin, A. G.; Kruglov, I. A.; Oganov, A. R. Actinium hydrides AcH₁₀, AcH₁₂, and AcH₁₆ as high-temperature conventional superconductors. *J. Phys. Chem. Lett.* **2018**, *9*, 1920–1926.
- (31) Wierzbowska, M.; de Gironcoli, S.; Giannozzi, P. Origins of low- and high-pressure discontinuities of T_c in niobium. *arXiv e-prints*, 2005, cond-mat/0504077.
- (32) Allen, P. B.; Dynes, R. C. Transition temperature of strongly-coupled superconductors reanalyzed. *Phys. Rev. B* **1975**, *12*, 905–922.
- (33) Palatinus, L.; Chapuis, G. SUPERFLIP—a computer program for the solution of crystal structures by charge flipping in arbitrary dimensions. *J. Appl. Crystallogr.* **2007**, *40*, 786–790.
- (34) Petříček, V.; Dušek, M.; Palatinus, L. Crystallographic computing system JANA2006: general features. *Z. Kristallogr. Cryst. Mater.* **2014**, *229*, 345–352.